Real-Space Visualization of Charged Polymer Network of Hydrogel by Double Network Strategy and Mineral Staining

Shinji Noguchi,[1] Ryuji Kiyama,[2,3] Masahiro Yoshida,[4] Maradhana Agung Marsudi,[4] Naohiro Kashimura,[4] Kiyoharu Tadanaga,[5] Jian Ping Gong,[2,6] and Takayuki Nonoyama[2]*

[1]Graduate School of Chemical Sciences and Engineering, Hokkaido University, Kita-13, Nishi-8, Kita-ku, Sapporo 060-8628, Japan

[2]Faculty of Advanced Life Science, Hokkaido University, Kita-21, Nishi-11, Kita-ku, Sapporo 001-0021, Japan

[3]Laboratoire de Sciences et Ingénierie de la Matière Molle, CNRS, ESPCI Paris, PSL Research University, 10 rue Vauquelin, 75005 Paris, France

[4]Graduate School of Life Science, Hokkaido University, Kita-21, Nishi-11, Kita-ku, Sapporo 001-0021, Japan

[5]Faculty of Engineering, Hokkaido University, Kita-13, Nishi-8, Kita-ku, Sapporo, 060-8628, Japan

[6]Institute for Chemical Reaction Design and Discovery (WPI-ICReDD), Hokkaido University, Kita-21, Nishi-11, Kita-ku, Sapporo 001-0021, Japan

KEYWORDS: Analytical methods, Electron microscopy, Gels, Nanostructure, Polymers

ABSTRACT:

Hydrogels consist of 3D and complicated polymer networks that determine their physical properties. Among the methods for structural analyses of hydrogels, the real-space imaging of a polymer network of hydrogel on a nanometer scale is one of the optimal ones; however, it is highly challenging. In this study, we propose a direct observation method for cationic polymer networks using transmission electron microscopy (TEM). By combining the double network strategy and the mineral staining technique, we overcame the challenges of polymer aggregation and the low electron density of the polymer. An objective cationic network was incorporated into a neutral skeleton network to suppress shrinkage during subsequent staining. Titania mineralization along the cationic polymer strands provided sufficient electron density for the objective polymer network for TEM observation. This observation method enables the visualization of local structures in real space and plays a complementary role to scattering methods for soft matter structure analysis.

Main content

Hydrogels consist of three-dimensional nanoscale polymer networks that store large amounts of water. Owing to their unique structure, hydrogels possess both solid and liquid characteristics such as elasticity[1,2] and solute diffusion capability.[3,4] Synthetic hydrogels have been widely used in various fields such as water-absorbent paper diapers,[5,6] ice packs,[7] and contact lenses.[8] Moreover, advanced hydrogels possessing extraordinarily high mechanical strength and toughness have been recently developed, which are promising for applications as load-bearing biomaterials, such as artificial cartilage.[9–12] The mechanical properties of hydrogels are governed by their polymer network structures. Static and dynamic scattering (light,[13] X-ray,[14] or neutron[15]) techniques are often employed to evaluate the structure from nano to microscale, which allows us to observe the "average" structure of the polymer network.[16,17] However, synthetic hydrogels inevitably possess a hierarchical inhomogeneous network structure, and certain properties such as fracture and subsequent crack propagation strongly depend on the "local" structure. Therefore, the local structure is essential for predicting such a phenomenon, and ideal methods for analysis are required.

The most straightforward method for analyzing the structure is direct observation in real space. Mesh size is one of the fundamental parameters of hydrogels and is generally in the range of several tens of nanometers.[18,19] Atomic force microscopy (AFM) and transmission electron microscopy (TEM) are available for real-space observations at such scales. Modern atomic force microscopes have an angstrom-scale resolution to distinguish individual atoms and enable us to observe the shape of a supermolecule,[20–23] the structure of proteins,[24] or the molecular shape before and after a chemical reaction[25] in ambient or underwater environments. In addition, the AFM capturing molecular motion has been developed.[26,27] However, observing individual polymer

strands in a hydrogel is difficult because of their fast Brownian motion. TEM enables us to observe specimens in a similar range of scales as AFM; however, aqueous solvents are not directly applicable because of the high vacuum conditions required by TEM. Water molecules in the gel sample must be exchanged for resin or non-volatile solvents such as ionic liquids without any structural changes.[28] Moreover, the conventional hydrogel network, which consists of light elements such as C, N, O, and H, must be stained. The general method to enhance the electron density is electron staining with heavy element compounds such as uranyl acetate[29,30] and phosphotungstic acid.[31,32] Although this method allows the observation of self-assembled peptide nanofibers[33–35] and refolded spherical protein complex networks,[36] direct visualizations of individual polymer chains within synthetic hydrogels have not been achieved using this approach. Synthetic polymer strands are thin, flexible, and susceptible to aggregation during staining or resinification. Thus, the structural information at the mesh size scale is lost during sample preparation.

We recently developed a method for visualizing anionic polymer network structures using TEM in a vacuum.[37] This method combines two techniques: mineral staining and double networking. Mineral staining is the selective mineralization of polyelectrolytes, which enhances electron density. By exploiting the substance diffusion capability of hydrogels, mineral formation on the polymer strands of the gel can be achieved.[38] When the mineral source ions diffuse into the polyelectrolyte gel, the charged group of the polymer side chain initiates mineral formation, known as heterogeneous nucleation and mineral growth is guided along the polymer chain under mild conditions to replicate the network structure. However, polyelectrolyte hydrogels usually shrink when soaked in saline solutions with high ionic strength.[17,39] In addition to shrinkage, the polymer strands aggregate by mineral deposition. Double networking is an ideal solution for preserving the

structure of the objective charged polymer network during mineral staining.[40,41] When another neutral polymer network with a relatively high concentration interpenetrates the target polyelectrolyte network, the neutral network works as an additional osmolyte in the target gel and compensates for the osmotic pressure lost by the salt solution. Moreover, this neutral network is chemically inert during the mineralization reaction. Consequently, the isovolumetric mineralization of the target polyelectrolyte can be achieved. This neutral network is called a skeleton network. In a previous study, the objective network and mineral were negatively charged polymers and ferric oxide, respectively.

The purpose of this research was to develop a real-space visualization of cationic polymer network structures using TEM. As shown in **Figure 1**, Cationic poly ([3-(methacryloylamino)propyl] trimethylammonium chloride) (PMPTC), neutral polydimethylacrylamide (PDMAAm), and titanium dioxide (TiO_2) were used as the objective polymer network, skeleton network, and staining mineral, respectively. Poly (*N,N*-Dimethylamino propyl acrylamide, methyl chloride quaternary) (PDMAPAA-Q) and poly (*N,N*-Dimethylamino ethyl acrylate, benzyl chloride quaternary) (PDMAEA-BQ) were also used as a cationic polymer for confirming mineralization along the cationic polymer. The anionic polymer, poly(2-Acrylamido-2-methylpropane sulfonic acid) (PAMPS), and the zwitterionic polymer, poly (*N*-(carboxymethyl)-*N*,*N*-dimethyl-2-(methacryloyloxy) ethanaminium) (PCDME), were also employed as an objective network for the control samples. **Figure 1** shows the conceptual illustration of real-space observation of the cationic polymer network of a hydrogel using TEM. First, the target PMPTC single network (SN) gel was synthesized via free radical polymerization. To preserve its structure, the PDMAAm skeleton network was polymerized in the presence of a PMPTC network. This double network (DN) gel was immersed in a titanium bis (ammonium

lactate) dihydroxide (TBALDH) solution to mineralize titanium dioxide on the PMPTC network via the catalytic effect of the cationic tertiary amine group.[42–45] Finally, the gel was resinified without any volume change or phase separation using a good-affinity resin solvent. Thus, the polymer network structure can be visualized via TEM of the titanium dioxide network. The detail of hydrogel preparation and mineralization was shown in **supporting information**.

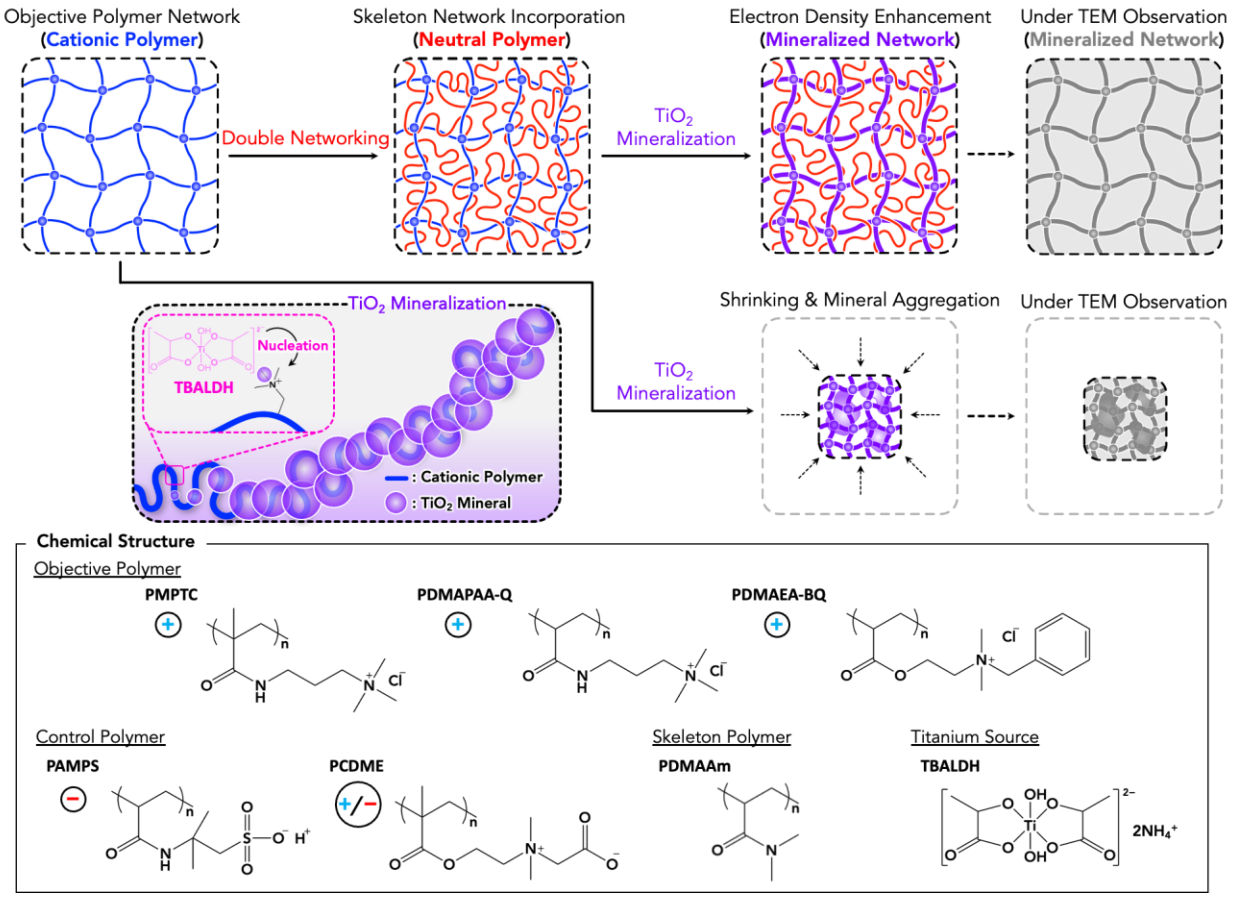

Figure 1. Chemical structures and concept of real-space observation of the cationic polymer network of the hydrogel by the combination of double networking and mineral staining techniques.

The mineralization from the titanium source solution was performed in various objective networks (cationic, anionic, and neutral) to confirm the catalytic effect on TiO_2 formation. **Figure 2a** shows the appearance of SN and DN gels before and after mineralization. All gels were transparent in the pristine state. After immersion in the TBALDH solution, the PMPTC SN and PMPTC/PDMAAm DN gels became opaque white, while the PAMPS/PDMAAm DN and PDMAAm SN gels remained transparent, indicating that only the PMPTC hydrogels containing cationic moieties possessed the capability to catalyze mineralization from the titanium source. It is important that the PDMAAm SN gel did not show mineral deposition, meaning this neutral network is suitable because the skeleton network is invisible under TEM. Comparing the cationic SN gel with the DN gel, the SN gel showed large shrinkage (volume ratio Q = 0.6), whereas the volume change in the DN gel was almost negligible owing to the skeleton effect of the PDMAAm network (Q = 1.0). The anionic PAMPS/PDMAAm DN gel also showed less volume change (Q = 1.0) but did not possess mineralization capability. From thermogravimetric differential thermal analysis (TG/DTA), the amount of minerals in the mineralized PMPTC/PDMAAm DN gel was approximately 5 wt% (**Figure S1**). The small minority of components was ideal for visualizing individual polymer strands without aggregated artifacts. Because of the small amount of mineral deposition in the gel, it was difficult to obtain crystalline information by X-ray diffraction (XRD) from the wet hydrogel. **Figure 2b** shows that all the hydrogels showed a broad peak corresponding to water.[46] When the ash obtained from sintering-mineralized hydrogel samples at 400 ^{o}C was measured, the PMPTC/PDMAAm DN gel showed anatase peaks, indicating that the cationic PMPTC polymer possesses TiO_2 mineralization capability, and the phase of mineralized TiO_2 was amorphous in the wet hydrogel state.

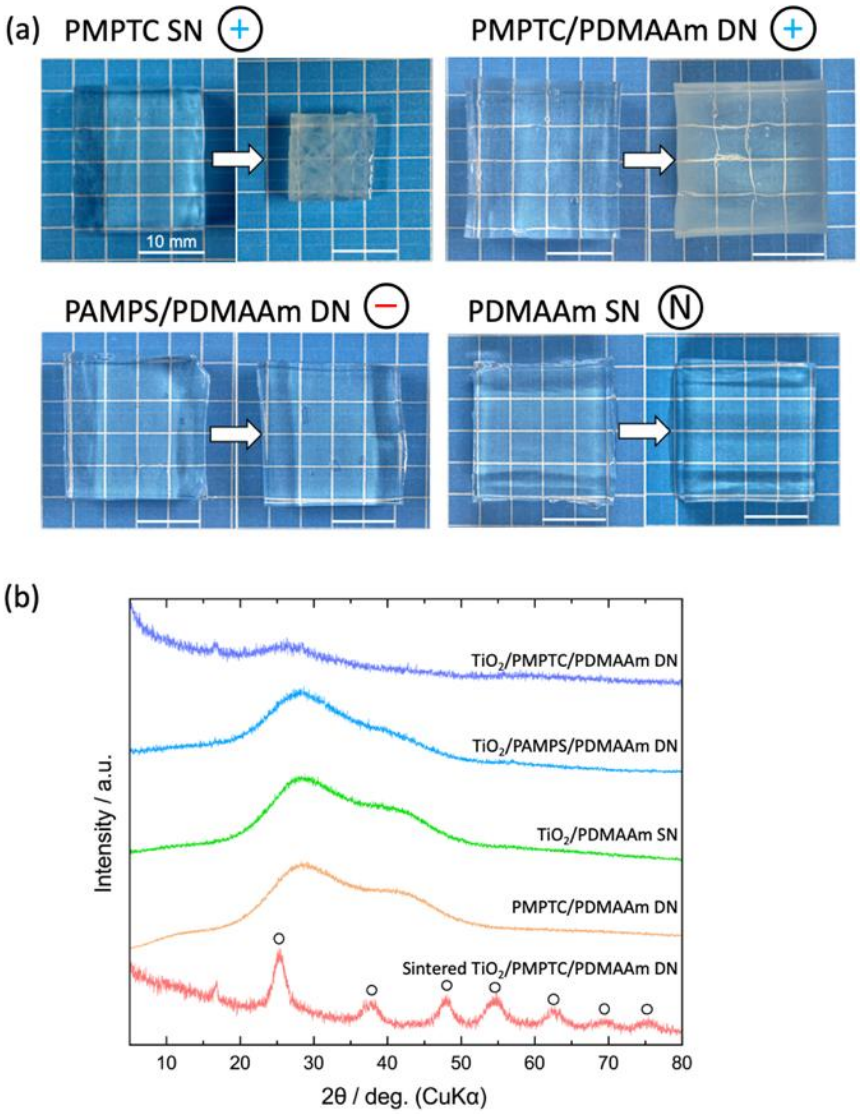

Figure 2. (a) Hydrogels before and after the TiO_2 mineralization. The cross-linker concentration of the first network is fixed at 5 mol% in all samples. The volume swelling ratio Q of each gel was 0.6 (PMTC SN), 1.0 (PMPTC/PDMAAm DN), 1.0 (PAMPS/PDMAAm DN), and 1.0 (PDMAAm SN). (b) XRD profiles of hydrogels and ash obtained from calcification of PMPTC/PDMAAm DN. The circle symbols were assigned to the anatase phase.

Next, to visualize the morphology of hydrogel, TEM observations of the mineralized hydrogels were performed. The water in the gel was gradually replaced with a curing reagent according to a previously developed method.[37] When the PDMAAm polymer was adopted as the skeleton network, volume changes and phase separation were not observed, even after curing.[37] **Figure 3a–c** show the TEM images of the TiO_2 mineralized gels with different cationic polymers as the objective network. Network morphology was clearly observed in the PMPTC/PDMAAm DN, PDMAPAA-Q/PDMAAm DN, and PDMAEA-BQ/PDMAAm DN gels. As indicated by X-ray scattering analysis,[16,17] the observed network had an inhomogeneous structure. Lattice fringes were not observed in the high-magnification TEM images of the PMPTC/PDMAAm DN gels (**Figure S2**). This result supports that the formed titanium dioxide was amorphous. To further support the mineral visualization results of the polymer network structure, PMPTC/PDMAAm DN gels with different PMPTC network densities were observed using TEM (**Figure 3a, d, e**). The network density was tuned by changing the concentration of the cross-linker when the PMPTC network was polymerized. When the network density decreased, the visualized structure became sparser and the length of the continuous network strands became shorter. Compared to the denser 5 mol% cross-linker concentration, individual strands and branching structures corresponding to the cross-linking points were distinctly visible in the 1 and 3 mol% samples. The polymer network was distributed isotropically in three dimensions, whereas the structure in the thickness direction was only 100 nm because of microtome processing. Therefore, if the size of the network loop in the low-crosslinking gels is larger than the thickness of the specimen slice, it is cut off and resembles an incomplete network. Based on the TEM images, the mesh sizes of each gel increased with decreasing cross-linker concentration. This trend qualitatively agrees with that of the mesh sizes determined by the elastic modulus: 11 nm at 5 mol%, 30 nm at 3 mol%, and 95 nm at 1 mol%

(**Figure 3f**). Despite using the same cross-linker concentration (3 mol%), differences in the density of the visualized network structure of the PMPTC/PDMAAm DN gels, PDMAPAA-Q/PDMAAm DN gels, and PDMAEA-BQ/PDMAAm DN gels were noted. This variation is believed to be caused by differences in swelling degree, which stem from variations in reactivity with the crosslinking agent. When MPTC and DMAAm were copolymerized with the objective network containing 25% MPTC, a network structure with lower contrast was observed compared to networks formed from only PMPTC as the objective network (**Figure S3**). When the MPTC content in the objective network was reduced to 10% or less, the network structure became nearly imperceptible. This phenomenon is likely due to the decrease in the copolymerization ratio of MPTC, resulting in fewer sites for TiO_2 formation, and thus, insufficient amounts of TiO_2 are formed to provide adequate contrast for TEM observation. In contrast, a small number of aggregated particles, which were several nanometers in size, were observed in the PAMPS/PDMAAm DN gels (**Figure 3g**), and almost no specific structures were observed in the PCDME/PDMAAm DN gels (**Figure 3h**), and the PDMAAm SN gels (**Figure 3i**). These results confirm the formation of TiO_2 particles along the cationic objective polymer network chain in the DN gels. In addition, large-scale inhomogeneous structures of ~200 nm were observed in the PMPTC/PDMAAm DN gel with 5 mol% cross-linker (**Figure S2**).[47] Such microscopic structures, which are larger than the primary mesh size, can be distinctly visualized using this method.

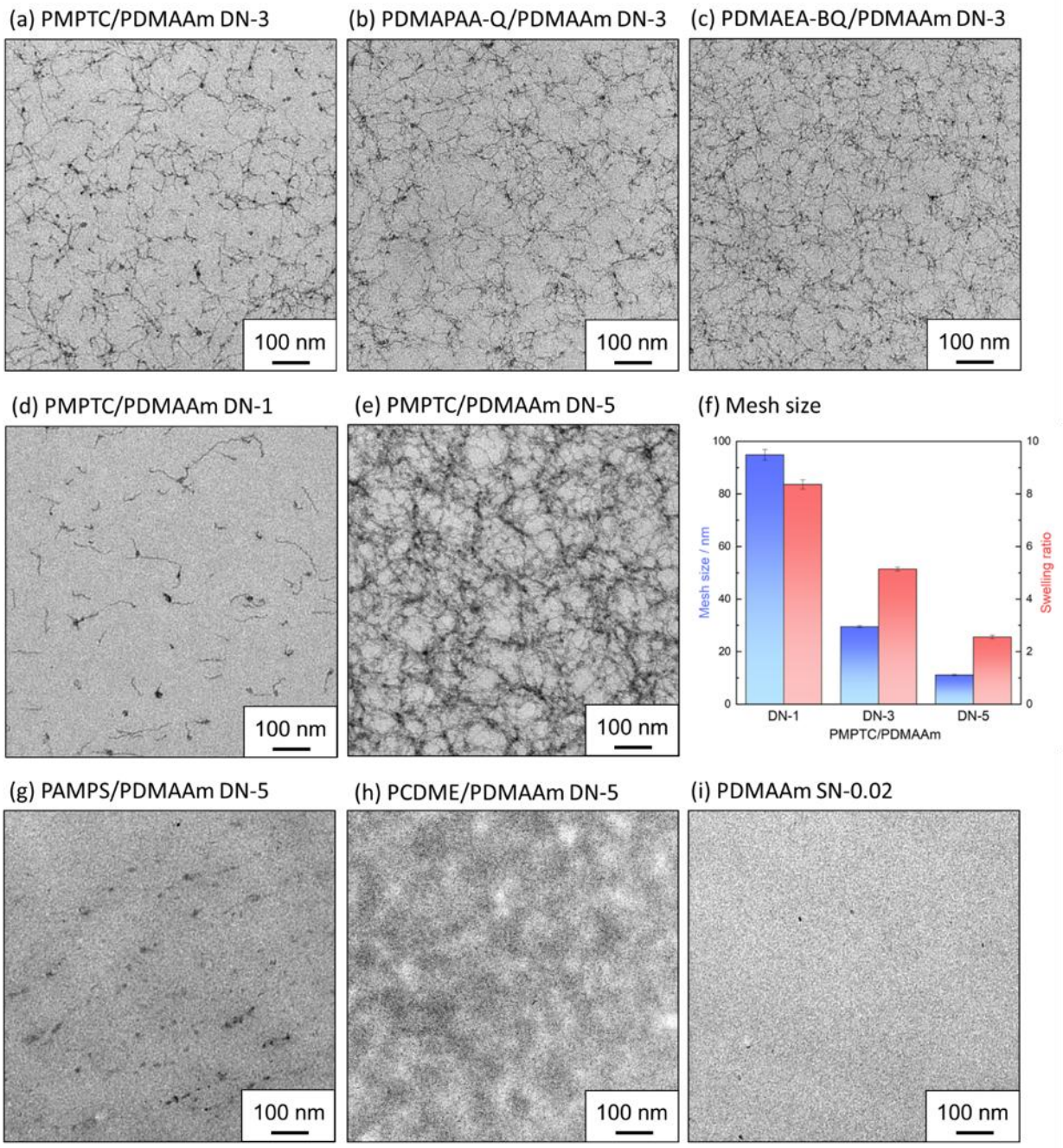

Figure 3. (a-e, g-i) TEM images of TiO_2 mineralized hydrogels. The numbers in the sample name show the cross-linker concentration [mol%] of each first network. (f) Mesh sizes and swelling ratios of DN gels of PMPTC/PDMAAm with different cross-linker concentrations in the first network.

To further analyze the mineralized network structure, scanning transmission electron microscopy (STEM) was conducted to acquire more detailed images at higher magnifications and elemental profiles. **Figure 4a–c** show high-angle annular dark-field (HAADF) STEM images of TiO_2 mineralized PMPTC/PDMAAm DN gels. Owing to the HAADF principle, the contrast of the TiO_2 improved, resulting in individual polymer strands, which were distinctly visible. The strand image consisted of the particles. The average thickness of the observed strand was 10 nm in case of the PMPTC/PDMAAm DN gel with 5 mol% cross-linker. Because the polymer strand typically winds in a high-entropy state, as shown in **Figure 1**, the mineral thickness may originate from the amplitude of flexion of the main chain. Ti was detected at the point of the formed particle with STEM-energy dispersive X-ray spectroscopy (EDX). In contrast, there is no Ti in the area outside of the particles. These results indicate that the observed mineral particles consisted of Ti minerals.

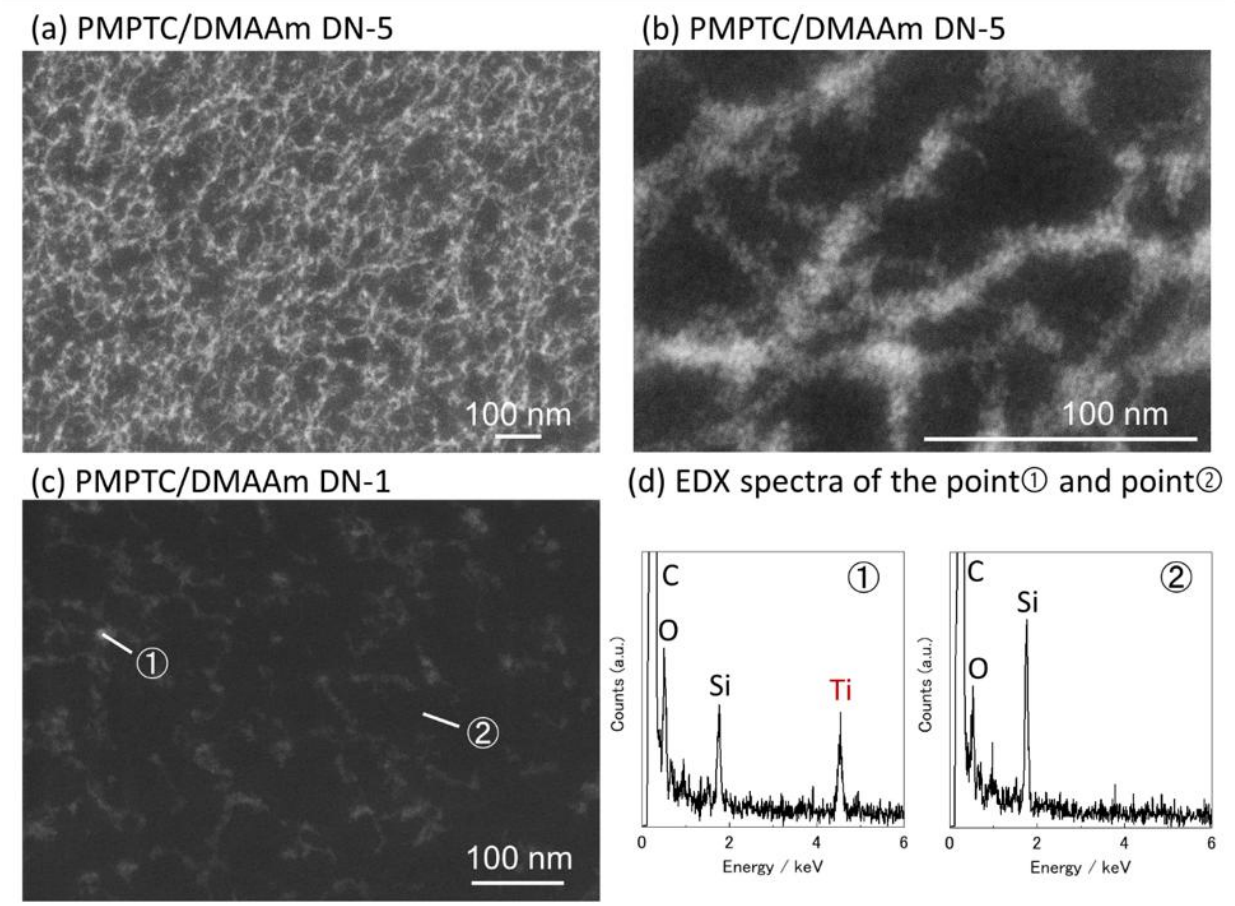

Figure 4. HAADF-STEM images of TiO_2/DN gels of PMPTC/ PDMAAm; (a) low magnification image, (b) high magnification image of 5 mol% cross-linker gel. (c) 1 mol% cross-linker gel image, and (d) EDX spectra of (c): i. a white point and ii. black point. Si signal is originated from the resin additive.

The obtained TEM images were divided into 50 nm vertically and horizontally, and the thickness of the polymer chain spanning the horizontal lines was analyzed (**Figure S4**). **Figure 5a** shows the width distributions of the strand object observed in TEM. The average width of the polymer chains at crosslinking agent concentrations of 1, 3, and 5 mol% was 5.6, 6.8, and 10.8 nm,

respectively. These values are much larger than that of the maximum side chain length (1.7 nm) calculated with bond length.[48] Because the polymer strand typically winds in a high-entropy state, as shown in **Figure 5b**, the mineral thickness originates from the amplitude of folding of the main chain. Polymer chains are considered to possess a fractal structure. When relatively weak tension is applied to the polymer strands, the larger structures unfold while the smaller structures remain unaffected. With increasing tension, even smaller structures are affected and unfold. Namely, the folding size of the polymer strands is related to the applied tension. When TiO_2 particles are formed on the polymer strands, larger folding sizes (i.e., lower tension) result in more flexible polymer chains that can aggregate more minerals, leading to the formation of larger TiO_2 particles. Under higher tension, the aggregation force of the minerals counteracts this tension, resulting in the formation of smaller particles. Therefore, the width of the minerals observed by TEM can be considered to indirectly visualize the local tension applied to the polymer strands within the gel network. The width distribution in **Figure 5a** indicates that higher cross-linker concentrations result in greater network inhomogeneity, which in turn leads to looser networks that do not effectively contribute to tension. Note that in samples with high cross-linking concentrations (5 mol%, **Figure 3e**), the network size may be too dense, resulting in some inter-chain aggregation, forming giant aggregates that are not dependent on chain tension.

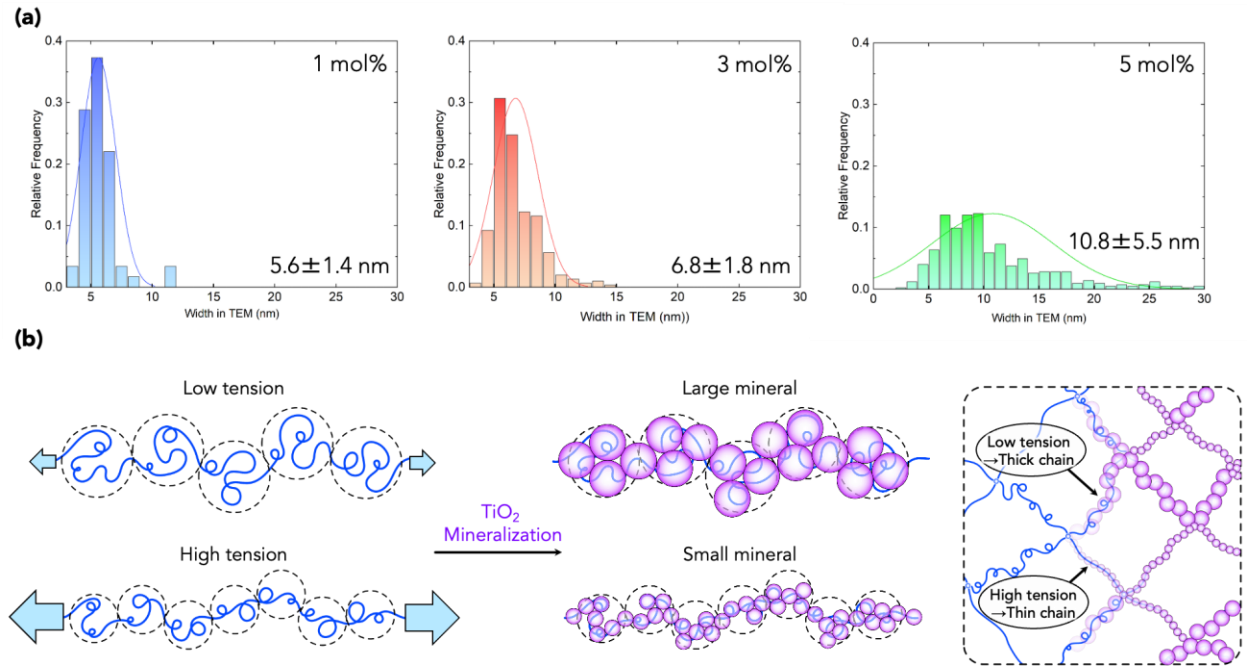

Figure 5. (a) Width distributions of the strand object observed in TEM. The median and deviation were obtained from Gaussian fitting. The network with a lower cross-linker concentration showed smaller width and deviation. It is mentioned that the Gaussian fitting is just shown for ease of viewing, and the actual distribution of the network structure in enough swollen gel usually does not follow a Gaussian distribution. (b) Relationship between the tension applying strand and the mineral size. The larger the tension is, the smaller the local structure is deformed. The cohesive force when mineral growing is competitive with the tension, resulting in the mineral size being smaller with increasing tension. In the inhomogeneous network, the variety of width observed in TEM is due to the tension distribution.

Furthermore, hydrogels can be considered as reaction media in liquid-phase synthesis for controlling the morphology of inorganic compounds through the utilization of functional groups. By employing double network formation and the selection of specific functional groups, titanium

dioxide was formed along the network structure of polymer chains. This material can be used as a photocatalyst, and when its dye degradation capability was compared, the TiO_2/DN gels demonstrated more than double the efficiency of amorphous titanium dioxide powder of the same weight (**Figure S5**). As indicated by the analytical results of the strand's width of polymer chains, the size of the synthesized inorganic compounds can be controlled by adjusting the tension of polymer chains through the concentration of cross-linking agents. Hydrogels serve as a means to synthesize inorganic compounds with novel forms and functionalities that have not been discovered in existing studies.

From the above results, the combination of TiO_2 mineral staining and double networking can visualize not only the single strands of the cationic polymer network of the hydrogel at the nanoscale but also the inhomogeneous network structures at the microscale under TEM observation. To date, the polymer chain structure of hydrogels has been inferred by mechanical tests and optical properties; however, by imaging the polymer chains, the physical properties of hydrogels can be confirmed in more detail. This observation method plays a complementary role to scattering methods for soft matter structure analysis. We believe this strategy enables the local analysis of hydrogel structure and leads to the elucidation of the origin of the physical properties of soft matter.

ASSOCIATED CONTENT

Supporting Information.

(0) Experimental section; (1) TG-DTA curves of gels before and after titanium oxide mineralization; (2) High-magnification TEM images of titanium oxide mineralized gels, electron diffraction images, and void structures; (3) TEM images of titanium oxide mineralized gels of copolymer; (4) Measurement points of the strand object width observed in TEM; (5) SEM image and XRD profile of amorphous TiO_2 used as a comparison target to TiO_2/DN gel for photocatalytic activity evaluation, and test results of dye degradation capability; The authors have cited additional references within the Supporting Information.[49,50] (PDF)

AUTHOR INFORMATION

Corresponding Author

Takayuki Nonoyama

[2]Faculty of Advanced Life Science, Hokkaido University, Kita-21, Nishi-11, Kita-ku, Sapporo 001-0021, Japan; Orcid: http://orcid.org/0000-0001-8554-0636; Email: nonoyama@sci.hokudai.ac.jp

Author

Shinji Noguchi

[1]Graduate School of Chemical Sciences and Engineering, Hokkaido University, Kita-13, Nishi-8, Kita-ku, Sapporo 060-8628, Japan; Orcid: https://orcid.org/0000-0003-1546-9998; Email: shinji@eis.hokudai.ac.jp

Ryuji Kiyama

[2]Faculty of Advanced Life Science, Hokkaido University, Kita-21, Nishi-11, Kita-ku, Sapporo 001-0021, Japan

[3]Laboratoire de Sciences et Ingénierie de la Matière Molle, CNRS, ESPCI Paris, PSL Research University, 10 rue Vauquelin, 75005 Paris, France

Masahiro Yoshida

[4]Graduate School of Life Science, Hokkaido University, Kita-21, Nishi-11, Kita-ku, Sapporo 001-0021, Japan

Maradhana Agung Marsudi

[4]Graduate School of Life Science, Hokkaido University, Kita-21, Nishi-11, Kita-ku, Sapporo 001-0021, Japan

Naohiro Kashimura

[4]Graduate School of Life Science, Hokkaido University, Kita-21, Nishi-11, Kita-ku, Sapporo 001-0021, Japan

Kiyoharu Tadanaga

[5]Faculty of Engineering, Hokkaido University, Kita-13, Nishi-8, Kita-ku, Sapporo 060-8628, Japan; Orcid: https://orcid.org/0000-0002-3319-4353; Email: tadanaga@eng.hokudai.ac.jp

Jian Ping Gong

[2]Faculty of Advanced Life Science and [5]Institute for Chemical Reaction Design and Discovery (WPI-ICReDD), Hokkaido University, Kita-21, Nishi-11, Kita-ku, Sapporo 001-0021, Japan; Orcid: http://orcid.org/0000-0003-2228-2750; Email: gong@sci.hokudai.ac.jp

Author Contributions

- Shinji Noguchi led the study, including conceiving the study idea, developing the experimental plan, conducting the experiments, drafting the original manuscript, and securing a portion of the research funding.

- Ryuji Kiyama contributed to the conception of the study, assisted in developing the experimental plan, and conducted some of the experiments.

- Masahiro Yoshida participated in conducting some of the experiments.

- Maradhana Agung Marsudi contributed to the conception of the study.

- Naohiro Kashimura provided guidance for some of the experiments.

- Kiyoharu Tadanaga provided guidance for specific experiments and supervised the execution of certain study aspects.

- Jian Ping Gong contributed to the conception of the study, secured a portion of the research funding, and supervised certain aspects of the study.

- Takayuki Nonoyama played a multifaceted role, including conceiving the study idea, developing the experimental plan, conducting experiments, securing a portion of the research funding, and overseeing the entire study's execution.

All authors reviewed the manuscript draft and revised it critically on intellectual content. All authors approved the final version of the manuscript to be published.

Funding Sources

- JST FOREST (Grant Nos. JPMJFR201Q)
- JST SPRING (Grant Nos. JPMJSP2119)
- JST ALCA-NEXT (Grant Nos. JPMJAN23C3)
- Grant-in-Aid for JSPS Fellows (No. 23KJ0014)
- KAKENHI (Grant Nos. JP22H04968, JP22K21342, 21H01990)
- Grant-in-Aid for Young Scientists (B) (No. 26820300)

Notes

The authors declare no competing financial interests.

ACKNOWLEDGMENT

Shinji Noguchi thanks Hokkaido University "Ambitious Leader's Program" supported by the Ministry of Education, Culture, Sports, Science and Technology (MEXT), Japan. This research was financially supported by FOREST (Grant Nos. JPMJFR201Q), SPRING (Grant Nos. JPMJSP2119), and ALCA-NEXT (Grant Nos. JPMJAN23C3) from the Japan Science and Technology Agency (JST), a Grant-in-Aid for JSPS Fellows (No. 23KJ0014), KAKENHI (Grant Nos. JP22H04968, JP22K21342), and Grant-in-Aid for Young Scientists (B) (No. 26820300) from the Japan Society for the Promotion of Science (JSPS). We thank the open facility of Hokkaido University Sousei Hall for the use of FE-TEM and STEM. Shinji Noguchi is grateful to Ms. Yuko Mori and Ms. Naomi Hirai of Hokkaido University for their support in electron microscopy analysis.

REFERENCES

(1) Xing, Z.; Lu, H.; Fu, Y. Q. Local Conservation Law of Rubber Elasticity in Hydrogel Networks Undergoing Microphase Separation and Toughening. *Polymer (Guildf)* **2021**, *222*, 123656. https://doi.org/10.1016/J.POLYMER.2021.123656.

(2) Wang, Y.; Fang, X.; Li, S.; Pan, H.; Sun, J. Complexation of Sulfonate-Containing Polyurethane and Polyacrylic Acid Enables Fabrication of Self-Healing Hydrogel Membranes with High Mechanical Strength and Excellent Elasticity. *ACS Appl Mater Interfaces* **2021**. https://doi.org/10.1021/acsami.1c21002.

(3) Liang, S.; Xu, J.; Weng, L.; Dai, H.; Zhang, X.; Zhang, L. Protein Diffusion in Agarose Hydrogel in Situ Measured by Improved Refractive Index Method. *Journal of Controlled Release* **2006**, *115* (2), 189–196. https://doi.org/10.1016/J.JCONREL.2006.08.006.

(4) Zheng, S.; Li, Z.; Liu, Z. The Fast Homogeneous Diffusion of Hydrogel under Different Stimuli. *Int J Mech Sci* **2018**, *137*, 263–270. https://doi.org/10.1016/J.IJMECSCI.2018.01.029.

(5) Abd Manan, T. S. B.; Beddu, S.; Mohamad, D.; Mohd Kamal, N. L.; Itam, Z.; Khan, T.; Jusoh, H.; Abdul Rahman, N. A.; Mohamed Nazri, F.; Mohd Yapandi, M. F. K.; Wan Mohtar, W. H. M.; Isa, M. H.; Che Muda, Z.; Ahmad, A.; Wan Rasdi, N. Physicochemical Properties of Absorbent Hydrogel Polymers in Disposable Baby Diapers. *Chem Phys Lett* **2021**, *774*, 138605. https://doi.org/10.1016/J.CPLETT.2021.138605.

(6) Bashari, A.; Rouhani Shirvan, A.; Shakeri, M. Cellulose-Based Hydrogels for Personal Care Products. *Polymers for Advanced Technologies*. John Wiley and Sons Ltd December 1, 2018, pp 2853–2867. https://doi.org/10.1002/pat.4290.

(7) Zou, J.; Wang, L.; Sun, G. Sustainable and Reusable Gelatin-Based Hydrogel “Jelly Ice Cubes” as Food Coolant. II: Ideal Freeze–Thaw Conditions. *ACS Sustainable Chemistry & Engineering* **2021**, *9* (46), 15365–15374. https://doi.org/10.1021/acssuschemeng.1c06309.

(8) Morgan, P. B.; Efron, N.; Helland, M.; Itoi, M.; Jones, D.; Nichols, J. J.; van der Worp, E.; Woods, C. A. Twenty First Century Trends in Silicone Hydrogel Contact Lens Fitting: An International Perspective. *Contact Lens and Anterior Eye* **2010**, *33* (4), 196–198. https://doi.org/10.1016/J.CLAE.2009.12.011.

(9) Chao, P. G.; Yodmuang, S.; Wang, X.; Sun, L.; Kaplan, D. L.; Vunjak-Novakovic, G. Silk Hydrogel for Cartilage Tissue Engineering. *J Biomed Mater Res B Appl Biomater* **2010**, *95* (1), 84–90. https://doi.org/10.1002/jbm.b.31686.

(10) Beck, E. C.; Barragan, M.; Tadros, M. H.; Gehrke, S. H.; Detamore, M. S. Approaching the Compressive Modulus of Articular Cartilage with a Decellularized Cartilage-Based Hydrogel. *Acta Biomater* **2016**, *38*, 94–105. https://doi.org/10.1016/J.ACTBIO.2016.04.019.

(11) Yang, F.; Zhao, J.; Koshut, W. J.; Watt, J.; Riboh, J. C.; Gall, K.; Wiley, B. J. A Synthetic Hydrogel Composite with the Mechanical Behavior and Durability of Cartilage. *Adv Funct Mater* **2020**, *30* (36). https://doi.org/10.1002/adfm.202003451.

(12) Nonoyama, T.; Gong, J. P. Annual Review of Chemical and Biomolecular Engineering Tough Double Network Hydrogel and Its Biomedical Applications. *The Annual Review of Chemical and Biomolecular* **2021**, *12*, 393–410. https://doi.org/10.1146/annurev-chembioeng.

(13) Zabashta, Y. F.; Kovalchuk, V. I.; Svechnikova, O. S.; Bulavin, L. A. APPLICATION OF THE LIGHT SCATTERING METHOD TO STUDY THE HYDROGEL SURFACE STRUCTURE. *Ukrainian Journal of Physics* **2022**, *67* (6), 463–467. https://doi.org/10.15407/ujpe67.6.463.

(14) Brey, E. M.; Appel, A.; Chiu, Y. C.; Zhong, Z.; Cheng, M. H.; Engel, H.; Anastasio, M. A. X-Ray Imaging of Poly(Ethylene Glycol) Hydrogels without Contrast Agents. *Tissue Eng Part C Methods* **2010**, *16* (6), 1597–1600. https://doi.org/10.1089/ten.tec.2010.0150.

(15) Endo, H.; Miyazaki, S.; Haraguchi, K.; Shibayama, M. Structure of Nanocomposite Hydrogel Investigated by Means of Contrast Variation Small-Angle Neutron Scattering. *Macromolecules* **2008**, *41* (14), 5406–5411. https://doi.org/10.1021/ma800390p.

(16) Shibayama, M. Spatial Inhomogeneity and Dynamic Fluctuations of Polymer Gels. *Macromol. Chem. Phys* **1998**, *199*.

(17) Rubinstein, M.; Ralph H, C. *Polymers Physics*; 2003; Vol. 23.

(18) Munoz-Pinto, D. J.; Samavedi, S.; Grigoryan, B.; Hahn, M. S. Impact of Secondary Reactive Species on the Apparent Decoupling of Poly(Ethylene Glycol) Diacrylate Hydrogel Average Mesh Size and Modulus. *Polymer (Guildf)* **2015**, *77*, 227–238. https://doi.org/10.1016/J.POLYMER.2015.09.032.

(19) Browning, M. B.; Wilems, T.; Hahn, M.; Cosgriff-Hernandez, E. Compositional Control of Poly(Ethylene Glycol) Hydrogel Modulus Independent of Mesh Size. *J Biomed Mater Res A* **2011**, *98 A* (2), 268–273. https://doi.org/10.1002/jbm.a.33109.

(20) Schappacher, M.; Deffieux, A. Imaging of Catenated, Figure-of-Eight, and Trefoil Knot Polymer Rings. *Angewandte Chemie - International Edition* **2009**, *48*, 5930–5933. https://doi.org/10.1002/anie.200900704.

(21) Schappacher, M. Synthesis of Macrocyclic Copolymer. *Science (1979)* **2008**, *319* (5869), 1512–1516. https://doi.org/10.1126/science.1153848.

(22) Deffieux, A.; Schappacher, M.; Hirao, A.; Watanabe, T. Synthesis and AFM Structural Imaging of Dendrimer-Like Star-Branched Polystyrenes. *J Am Chem Soc* **2008**, *130* (17), 5670–5672. https://doi.org/10.1021/ja800881k.

(23) Schappacher, M.; Deffieux, A. Atomic Force Microscopy Imaging and Dilute Solution Properties of Cyclic and Linear Polystyrene Combs. *J Am Chem Soc* **2008**, *130* (44), 14684–14689. https://doi.org/10.1021/ja804780s.

(24) Müller, D. J.; Janovjak, H.; Lehto, T.; Kuerschner, L.; Anderson, K. Observing Structure, Function and Assembly of Single Proteins by AFM. *Prog Biophys Mol Biol* **2002**, *79* (1–3), 1–43. https://doi.org/10.1016/S0079-6107(02)00009-3.

(25) de Oteyza, D. G.; Gorman, P.; Chem, Y.-C.; Wickenburg, S.; Riss, A.; Mowbray, D. J.; Etkin, G.; Peddrarazi, Z.; Tsai, H.-Z.; Rubio, A.; Crommie, M. F.; Fisher, F. R. Direct Imaging of Covalent Bond. *Science (1979)* **2013**, *340* (June), 1434–1437.

(26) TAKAYUKI UCHIHASHI; RYOTA IINO; TOSHIO ANDO; HIROYUKI NOJI. High-Speed Atomic Force Microscopy Reveals Rotary Catalysis of Rotorless F1-ATPase. *Science (1979)* **2011**, *333* (6043), 755–758. https://doi.org/10.1126/science.1205510.

(27) Fukui, T.; Uchihashi, T.; Sasaki, N.; Watanabe, H.; Takeuchi, M.; Sugiyasu, K. Direct Observation and Manipulation of Supramolecular Polymerization by High-Speed Atomic Force Microscopy. *Angewandte Chemie* **2018**, *130* (47), 15691–15696. https://doi.org/10.1002/ange.201809165.

(28) Newman, G. R.; Jasani, B.; Williams, E. D. *A Simple Post-Embedding System for the Rapid Demonstration of Tissue Antigens under the Electron Microscope*; 1983; Vol. 15.

(29) Stempak, J. G.; Ward, R. T. AN IMPROVED STAINING METHOD FOR ELECTRON MICROSCOPY. *The Journal of Cell Biology* **1964**, *22*, 697–701.

(30) And, J. B.; Cxtol, B. Staining of Tissue Sections for Electron Microscopy with Heavy Metals II. Application of Solutions Containing Lead and Barium*. *J Biophys and Biochem Cytol* **1958**, *4* (6), 727–730.

(31) Sheridan, W. F.; Barrnett, R. J. Cytochemical Studies on Chromosome Ultrastructure. *J Ultrastruct Res* **1969**, *27* (3–4), 216–229. https://doi.org/10.1016/S0022-5320(69)80013-4.

(32) Rocha, G. M.; Brandão, B. A.; Mortara, R. A.; Attias, M.; De Souza, W.; Carvalho, T. M. U. The Flagellar Attachment Zone of Trypanosoma Cruzi Epimastigote Forms. *J Struct Biol* **2006**, *154* (1), 89–99. https://doi.org/10.1016/J.JSB.2005.11.008.

(33) Nguyen, V. D.; Pal, A.; Snijkers, F.; Colomb-Delsuc, M.; Leonetti, G.; Otto, S.; Van Der Gucht, J. Multi-Step Control over Self-Assembled Hydrogels of Peptide-Derived Building Blocks and a Polymeric Cross-Linker. *Soft Matter* **2016**, *12* (2), 432–440. https://doi.org/10.1039/c5sm02088c.

(34) Chen, S.; Zhou, A.; He, B.; Zhao, W.; Chen, X.; Jiang, D. Designer D-Form Self-Assembling Peptide Scaffolds Promote the Proliferation and Migration of Rat Bone Marrow-Derived Mesenchymal Stem Cells. *Int J Mol Med* **2017**, *40* (3), 679–688. https://doi.org/10.3892/ijmm.2017.3056.

(35) Haines-Butterick, L.; Rajagopal, K.; Branco, M.; Salick, D.; Rughani, R.; Pilarz, M.; Lamm, M. S.; Pochan, D. J.; Schneider, J. P. Controlling Hydrogelation Kinetics by Peptide Design for Three-Dimensional Encapsulation and Injectable Delivery of Cells. *Proceedings of the National Academy of Sciences* **2007**, *104* (19), 7791–7796.

(36) Yamanaka, M.; Mashima, T.; Ogihara, M.; Okamoto, M.; Uchihashi, T.; Hirota, S. Construction of Ferritin Hydrogels Utilizing Subunit–Subunit Interactions. *PLoS One* **2021**, *16* (11), e0259052. https://doi.org/10.1371/journal.pone.0259052.

(37) Kiyama, R.; Yoshida, M.; Nonoyama, T.; Sedlačík, T.; Jinnai, H.; Kurokawa, T.; Nakajima, T.; Gong, J. P. Nanoscale TEM Imaging of Hydrogel Network Architecture. *Advanced Materials* **2022**, *2208902*, 2208902. https://doi.org/10.1002/adma.202208902.

(38) Nonoyama, T.; Wada, S.; Kiyama, R.; Kitamura, N.; Islam Mredha, M.; Zhang, X.; Kurokawa, T.; Nakajima, T.; Takagi, Y.; Yasuda, K.; Ping Gong, J.; Wada, S.; Kitamura, N.; Yasuda, K.; Kiyama, R.; I Mredha, M. T.; Zhang, X.; Takagi, Y. Double-Network Hydrogels Strongly Bondable to Bones by Spontaneous Osteogenesis Penetration. *Advanced Materials* **2016**, *28*, 6470–6475. https://doi.org/10.1002/adma.201601030.

(39) Shibayama, M. *Spatial Inhomogeneity and Dynamic Fluctuations of Polymer Gels*; 1998; Vol. 199.

(40) Gong, J. P.; Katsuyama, Y.; Kurokawa, T.; Osada, Y. Double-Network Hydrogels with Extremely High Mechanical Strength. *Advanced Materials* **2003**, *15* (14). https://doi.org/10.1002/adma.200304907.

(41) Nakajima, T.; Chida, T.; Mito, K.; Kurokawa, T.; Gong, J. P. Double-Network Gels as Polyelectrolyte Gels with Salt-Insensitive Swelling Properties. *Soft Matter* **2020**, *16*, 5487. https://doi.org/10.1039/d0sm00605j.

(42) Ahn, S.; Park, S.; Lee, S. Y. Oligo(L-Lysine)-Induced Titanium Dioxide: Effects of Consecutive Lysine on Precipitation. *J Cryst Growth* **2011**, *335* (1), 100–105. https://doi.org/10.1016/J.JCRYSGRO.2011.09.006.

(43) Nonoyama, T.; Kinoshita, T.; Higuchi, M.; Nagata, K.; Tanaka, M.; Sato, K.; Kato, K. TiO2 Synthesis Inspired by Biomineralization: Control of Morphology, Crystal Phase, and Light-Use Efficiency in a Single Process. *J Am Chem Soc* **2012**, *134* (21), 8841–8847. https://doi.org/10.1021/ja211347n.

(44) Seisenbaeva, G. A.; Daniel, G.; Nedelec, J.-M.; Kessler, V. G. Solution Equilibrium behind the Room-Temperature Synthesis of Nanocrystalline Titanium Dioxide. *Nanoscale* **2013**, *5* (8), 3330–3336. https://doi.org/10.1039/c3nr34068f.

(45) HernándezHern, A.; AndrésAndr, ab; HernándezHern, A.; Campero-Celis, A.; Irais Vera-Robles, L. TiBALDH as a Precursor for Biomimetic TiO 2 Synthesis: Stability Aspects in Aqueous Media. *RSC Adv* **2019**, *9* (59), 34559–34566. https://doi.org/10.1039/c9ra05923g.

(46) Fukao, K.; Nonoyama, T.; Kiyama, R.; Furusawa, K.; Kurokawa, T.; Nakajima, T.; Ping Gong, J. Anisotropic Growth of Hydroxyapatite in Stretched Double Network Hydrogel. *ACS Nano* **2017**, *11* (12), 12103–12110. https://doi.org/10.1021/acsnano.7b04942.

(47) Fukao, K.; Nakajima, T.; Nonoyama, T.; Kurokawa, T.; Kawai, T.; Gong, J. P. Effect of Relative Strength of Two Networks on the Internal Fracture Process of Double Network

Hydrogels As Revealed by in Situ Small-Angle X-Ray Scattering. *Macromolecules* **2020**, *53* (4), 1154–1163. https://doi.org/10.1021/acs.macromol.9b02562.

(48) Allen, F. H.; Kennard, O.; Watson, D. G.; Brammer, L.; Orpen, A. G.; Taylor, R. *Tables of Bond Lengths Determined by X-Ray and Neutron Diffraction. Part I. Bond Lengths in Organic Compounds's Close Bristol BS8 1 TS*.

(49) Schneider, C. A.; Rasband, W. S.; Eliceiri, K. W. NIH Image to ImageJ: 25 Years of Image Analysis. *Nature Methods*. July 2012, pp 671–675. https://doi.org/10.1038/nmeth.2089.

(50) McKee, C. T.; Last, J. A.; Russell, P.; Murphy, C. J. Indentation versus Tensile Measurements of Young's Modulus for Soft Biological Tissues. *Tissue Eng Part B Rev* **2011**, *17* (3), 155–164. https://doi.org/10.1089/ten.teb.2010.0520.

Table of Contents (ToC)